Pergamon

Int. J. Mech. Sci. Vol. 40, No. 7, pp. 683–694, 1998

Printed in Great Britain
0020-7403/98 $19.00 + 0.00

PII: S0020-7403(97)00089-1

THE CLAMPING STRESS IN A COLD-DRIVEN RIVET

X. DENG and J. W. HUTCHINSON
Division of Engineering and Applied Sciences, Harvard University, Cambridge, MA 01238, U.S.A.

Abstract—An analysis of a model of the process of cold-driving a rivet is carried out with the primary aim of identifying the origin and magnitude of the resulting clamping force exerted by the rivet on the lapped sheets. The development of high hydrostatic pressure in the rivet shank in the first stages of the driving process, and its subsequent release as the rivet head is squashed, is the key to understanding the origin of the clamping force. The average clamping stress in the rivet shank is on the order of $\sigma_Y/4$, where σ_Y is the yield stress of the rivet. The model is used to explore the role of some riveting variables, including differing yield stresses in the rivet and sheet materials, strain hardening, and head size. © 1998 Elsevier Science Ltd. All rights reserved

Keywords: cold-driven rivet, clamping force.

1. INTRODUCTION

The origin of the clamping force exerted on two sheets by a rivet that is driven hot and cooled is easy to understand and estimate, based on the thermal contraction of the shank relative to the sheets. By contrast, the origin of the clamping force in a rivet whose driving temperature is same as the sheets (i.e. "a cold-driven rivet") is not at all obvious. It is generally smaller in magnitude than the force in a hot-driven rivet and less easy to control [1]. The force exerted by the tool used to cold-drive rivets is known to have a significant effect on the fatigue life of riveted lap joints [2]. There is little doubt that the clamping force is in some way related to the driving force, and, further, that an increase in the rivet clamping force is responsible for the increase in fatigue life. Nevertheless, connections between the driving force and the clamping force have not been established. Indeed, there appears to be almost nothing in the technical literature on the mechanics of the clamping force of cold-driven rivets. Nor do there appear to be published efforts to measure clamping forces directly. It will be seen in this study that the mechanics of the clamping force is fairly subtle, requiring an understanding of the multi-axial stress history in the rivet during the riveting process. Simple arguments which invoke uniaxial stressing are unable to explain the origin of the clamping stress. Following the introduction of the model, an overview of the deformation stages will be given to guide the reader through the paper with emphasis on those stages in the process that are crucial to understand the origin of the clamping stress.

2. A MODEL FOR EXPLORING THE ORIGIN OF THE CLAMPING STRESS

The clamping stress is defined as the load exerted by the rivet in clamping two sheets together divided by the cross-sectional area of the shank at the interface between the sheets. The primary aim in this paper is to detail the development of the clamping stress in a cold-driven rivet and to obtain a reasonable approximation of its magnitude. In this spirit, the proposed model leaves out several features which will have to be taken into account in later work if more refined predictions are desired. The model does permit trends to be computed for dependence on some geometric parameters and on material properties of the rivet and sheet. A selection of such results will be presented at the end of the paper.

The geometry of the rivet and sheets at the start of the process is defined in Fig. 1, including a typical mesh in its undeformed state used in the numerical analysis. The same mesh in its deformed state at the end of the process is included in Fig. 1 to facilitate the discussion. Focus will be on an individual rivet. Interaction between rivets will be ignored. The geometry is axisymmetric and symmetric with respect to the plane ($z = 0$) separating the two sheets. Each sheet has thickness t. The initial radius of the rivet shank is R, and the cylindrical surface of the rivet is assumed to be in contact with the sheets at the start of the process. The unrealistic two-headed starting shape is

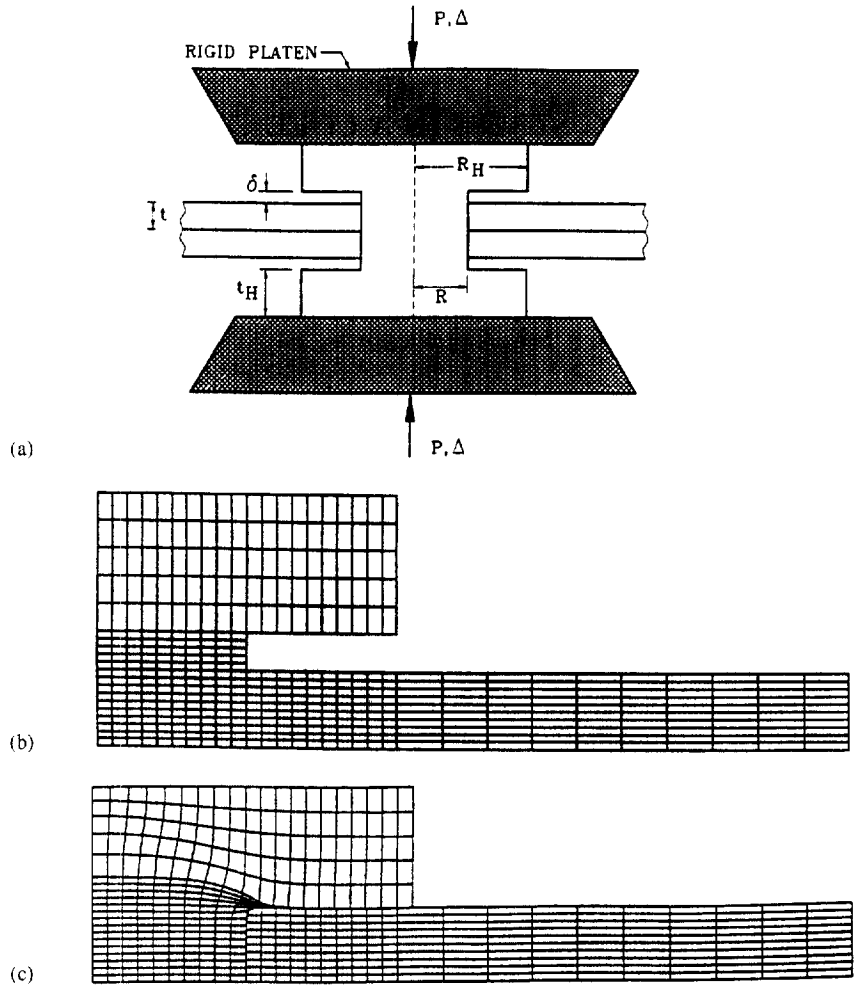

Fig. 1. (a) Undeformed geometry of the model. (b) Undeformed finite element mesh. (c) Same mesh as in (b) but in the deformed state with $\Delta/\delta = 1.25$. The proportions are correct for the example analyzed in Section 3 and presented in Figs 3–7. The rivet is driven by imposition of equal and opposite vertical displacements Δ of rigid, frictionless platens.

invoked to preserve symmetry about $z = 0$, which helps to isolate the essential mechanics as well as to reduce the computational effort required to analyze the model. This geometry also permits a meaningful small strain analysis of the process. By comparing small strain results with selected results from a finite strain analysis, it will be shown that finite strain effects are not essential to understand the origin of the clamping stress. The initial radius and thickness of the cylindrical rivet head are denoted by R_H, and t_H, respectively. The initial gap between the head and the sheet is taken to be δ, such that the entire initial length of the rivet shank is $2(t_H + \delta)$. Throughout the paper cylindrical coordinates (r, z) are used. At any stage in the process the average axial stress in the shank of the rivet at the mid-plane, $z = 0$, is given by

$$\bar{\sigma} = \frac{1}{\pi R^2} \int_0^R \sigma_{zz}\,(r, 0)\, 2\pi r\, dr. \tag{1}$$

Except for some results showing the effect of strain hardening given at the end of the paper, the rivet and sheet materials will be taken to be elastic–perfectly-plastic with an isotropic yield surface specified by the Mises stress invariant. The tensile yield stress of the sheet material is denoted by σ_Y and that of the rivet material by σ_Y^R. The materials are assumed to have the same Young's modulus, E, and Poisson's ratio, ν.

The rivet is loaded by imposing vertical driving displacements Δ of equal magnitude and opposite sign on the surface of the heads with no shear traction (Fig. 1). The effects of shear traction due to friction between the riveter and the rivet head will generally be small because most riveting processes involve repeated "hammering" of the rivet. The load P on the rivet is computed. During loading, when Δ is increasing, frictional effects between the rivet shank and the sheets are neglected and the shear traction along the interface is taken to be zero. During unloading, when the rivet head clamps the sheet, relative motion across the shank/sheet interface is suppressed, i.e. the interface is assumed to be "welded". Justification for these assumptions will be given later. The interface between the rivet head and the sheet is assumed to slide freely during the entire process. Selected calculations accounting for frictional contact on this interface will be cited that show the residual clamping force is insensitive to the condition assumed.

The model just described has been analyzed using the ABAQUS finite element code with eight-noded bi-quadratic axisymmetric quadrilateral elements. Most of the results have been computed within the small-strain framework, but selected results have been recomputed within a full finite-strain formulation. Six-noded axisymmetric interface elements are employed for the friction-free interface between the rivet head and the sheet and for the portion of the interface of the rivet shank not yet in contact with the sheet. The outer radius of the sheets is taken to be $11t$, ensuring that the stresses in the rivet will be essentially independent of this dimension of the model. The constitutive model is classical incremental plasticity (J_2 flow theory). For the elastic–perfectly-plastic solids, the plasticity is completely characterized by σ_Y and σ_Y^R. The stress–strain relation used for the hardening materials will be specified later in the paper.

To alert the reader on what to look for in reading the paper, a qualitative quide through the stages of the plastic *loading phase* of the riveting process is now provided. Five stages in the loading process are identified:

(A) Initial yield in the rivet shank;
(B) First contact between the rivet head and sheet;
(C) Attainment of maximum average axial compressive stress in rivet shank; (2)
(D) Squashing of the rivet head and release of compression in the shank;
(E) The limit stress state.

The top four sketches in Fig. 2 depict the geometry and the direction of material flow at three of the five stages. The bottom four sketches depict evolution as a function of the driving displacement Δ at the various stages of the loading process. Shown are the half-length of the shank, H, the radius of the head, R_H, the pressure, p, at the center of the shank, and the average compressive axial stress at the center plane of the shank, $-\bar{\sigma}$. Prior to contact between the rivet head and the sheet at (B), the axial compression in the shank is only slightly in excess of the yield stress. Once contact occurs, the sheets and shank experience extra constraint which causes the axial compression in the shank, $-\bar{\sigma}$, to increase to a peak at (C) of almost twice the yield stress, accompanied by a corresponding increase in the hydrostatic pressure, p. Until this point, the rivet head itself remains nominally elastic except where it joins the shank, and the overall direction of flow in the upper half of the rivet is directed downward. When the driving displacement Δ reaches the level required to begin squashing the rivet head at (D), the flow in head develops an outward radial component which in turn permits a release of much of the compression in the shank. This is the critical stage in the riveting process that ultimately produces a clamping stress. Material in the shank actually flows out of the hole during this stage, as depicted by the transient increase in H in Fig. 2(e). For an elastic–perfectly-plastic system, the limiting compressive stress in the shank, $-\bar{\sigma}$, in the loading phase ((E) in Fig. 2(i)) falls to roughly $3/4\,\sigma_Y$. The unloading phase (not shown, but discussed in the next section) adds a tensile component $\approx \sigma_Y$ across the center of the shank, leaving a residual clamping stress of roughly $1/4\sigma_Y$. Details are provided for a specific example in the next section.

It can be mentioned in passing that a small contribution to the clamping stress in a cold-driven rivet is produced from the temperature rise brought about by plastic deformation of the shank and the consequent thermal contraction when it cools. Most of the work of plastic deformation in the shank of the rivet appears as heat. Therefore, for an elastic–perfectly-plastic rivet material with yield stress, σ_Y, the temperature rise in the shank due to plastic work is approximately $\Delta T = \sigma_Y \varepsilon / c_V$, where c_V is its specific heat per unit volume and ε is the compressive plastic strain in the shank. When the shank cools, the resulting contribution to the clamping stress is given by $E\alpha\varepsilon\sigma_Y/c_V$, where E and

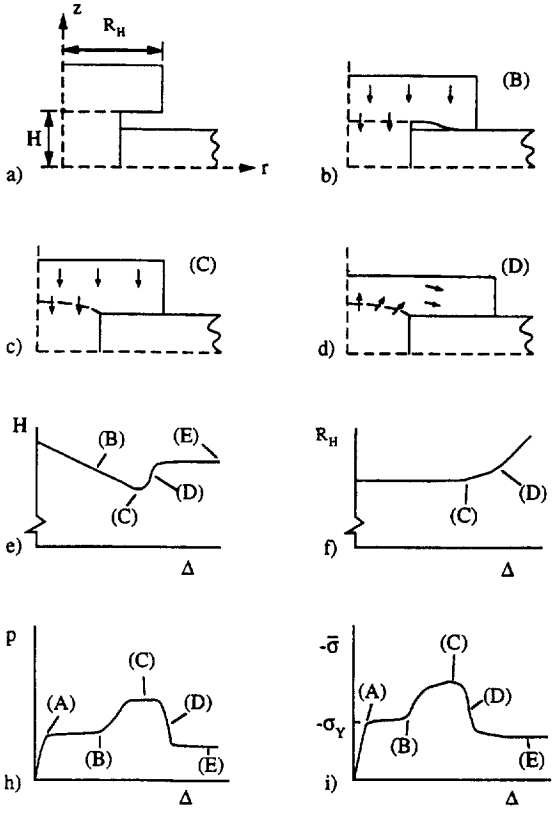

Fig. 2. A qualitative overview of the stages of the loading phase of the riveting process wherein Δ is increasing. The stages in the loading process, (A)–(E), are identified in Eqn (2). The arrows in parts (b)–(d) indicate the general direction of the material flow in the rivet.

α are the Young's modulus and coefficient of thermal expansion of the shank material. The compressive plastic strain in the shank itself does not exceed 10%, as will be seen. For a typical aluminum rivet material, this corresponds to a temperature rise ΔT of only several degrees centigrade and a clamping stress contribution of less than $\sigma_Y/20$. This thermal contribution will be neglected in the analysis which follows.

3. DETAILS OF STRESS DEVELOPMENT: A QUANTITATIVE EXAMPLE

In the example chosen to show quantitative details predicted by the model, the sheet and rivet materials are taken to be elastic–perfectly-plastic with a common tensile yield stress, σ_Y. The value $\sigma_Y/E = 0.005$ and $\nu = 0.33$ used in the computations correspond to an aluminum alloy with a yield stress of 50 ksi (345 MPa). The geometric ratio $R/t = 2$ is representative of that for an aircraft lap joint; in addition, the values $R_H/R = 2$ and $t_H/t = 1.75$ have been chosen for the example. The initial gap between the rivet head and sheet is taken to be $\delta/t = 0.5$. It will be seen subsequently that this choice for the initial gap gives rise to nearly the maximum possible clamping stress. The computations for this example, with one exception, have been carried out using the small strain formulation. The numerical results for this example are displayed in Figs 3–7, whose contents will be introduced and explained in some detail.

The plot of compressive load applied to the rivet P as a function of the driving displacement Δ is given in Fig. 3(a). A cross plot of P versus $\bar{\sigma}$ is given in Fig. 3(b). In each of these two plots, the solid curve denotes the loading portion of the history (with Δ monotonically increasing) and a dashed line represents unloading (with Δ decreasing after attaining Δ_{max}). Unloading to $P = 0$ from three values of Δ_{max} is illustrated. The residual value of $\bar{\sigma}$ at the end of the process when $P = 0$ is denoted by $\bar{\sigma}_{residual}$. A plot of the computed values of $\bar{\sigma}_{residual}/\sigma_Y$ as a function of Δ_{max}/δ is given in Fig. 4 (the

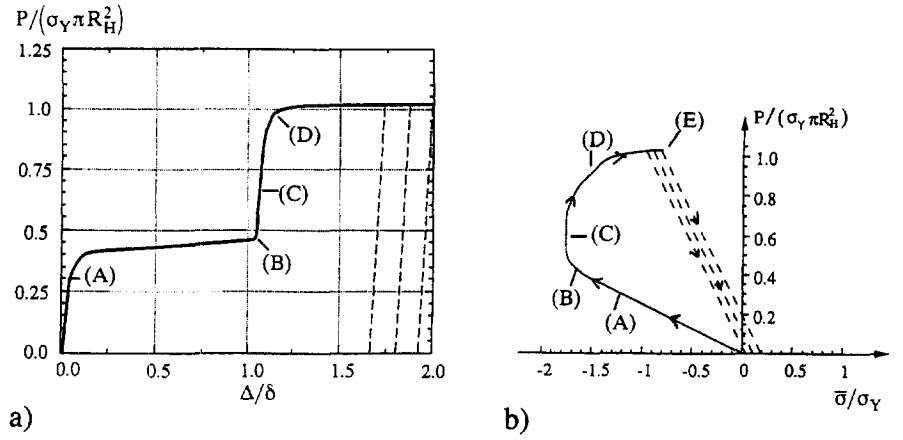

Fig. 3. (a) Load versus driving displacement. (b) Load versus average axial stress at the mid-plane of the rivet shank, $\bar{\sigma}$. The solid line curves denote the loading phase. The dashed line curves are associated with unloading from Δ_{max}. Unloading from three values of Δ_{max} are shown. The residual clamping stress is the value of $\bar{\sigma}$ at $P = 0$ in the unloading response. Identical rivet and sheet material properties with $\sigma_Y/E = 0.005$ and $\nu = 0.33$, and an undeformed geometry specified by $R/t = 2$, $\delta/t = 1/2$, $R_H/t = 4$ and $t_H/t = 1.75$. The stages in the loading process, (A)–(E), are identified in Eqn (2).

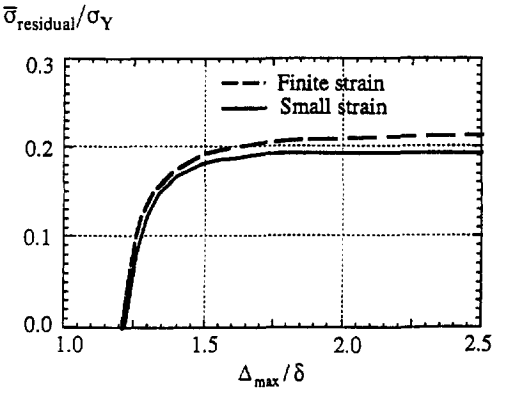

Fig. 4. Residual clamping stress at the mid-plane of the rivet shank as a function of the loading displacement at the onset of unloading, Δ_{max}. The limiting value approached, as Δ_{max} increases, is termed the *asymptotic residual cramping stress*. The parameters specifying the model are the same as those associated with the example in Fig. 3. Predictions from the finite-strain formulation are compared with those from the small-strain formulation.

finite strain results contained in this figure will be introduced later in the paper). The clamping force is given by $\pi R^2 \bar{\sigma}_{residual}$. To shed light on the behavior, we discuss these plots, supplementing them with additional stress distributions.

3.1. *The loading process*

The load P in Fig. 3 is normalized by $\sigma_Y \pi R_H^2$, which to a good approximation is the limit yield load of the rivet head (*E*). A limit load and the associated limiting stress distribution exist because a small-strain formulation is employed together with materials comprising the sheet and rivet which are elastic–perfectly-plastic. Initial yield in the rivet shank (A) occurs at a value of P slightly in excess of $\sigma_Y \pi R^2$ due to the lateral constraint of the sheets. Because friction between the shank and sheet is neglected during loading and because $(R/R_H)^2 = 1/4$ in this example, the slope of the normalized load versus average shank stress in Fig. 3(b) is exactly $-1/4$ before the head makes any contact with the sheet.

Between initial yield (A) and contact between the head and sheet (B), some shank material outside the sheet is forced into the rivet hole further compressing and radially expanding the shank, causing

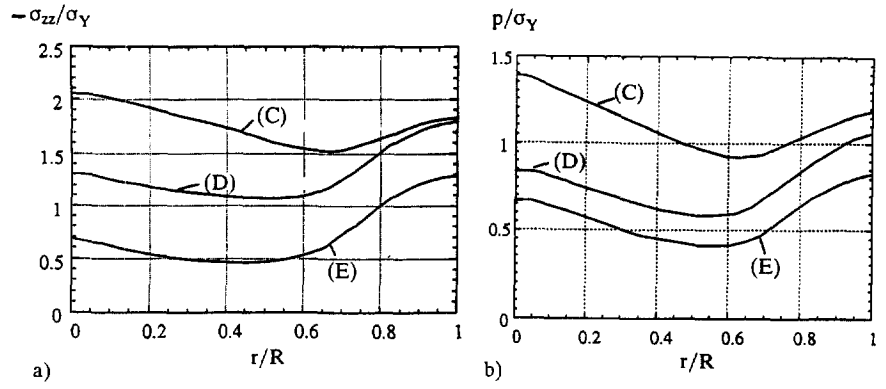

Fig. 5. Distribution of (a) the axial stress component, σ_{zz}, and (b) the hydrostatic pressure, p, across the mid-plane of the rivet shank at three stages of the loading process. See Eqn (2) for definitions of stages (C)–(E). The parameters specifying the model are the same as those associated with the example in Fig. 3.

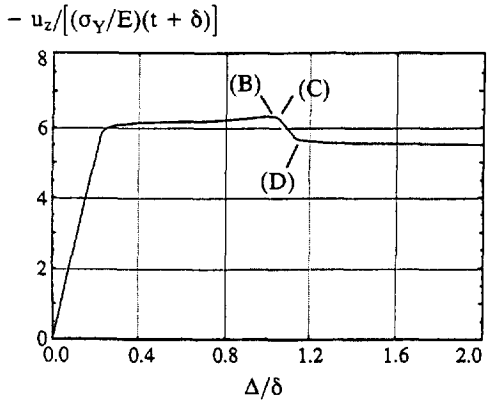

Fig. 6. Vertical displacement, u_z, at the center of the shank where it meets the upper rivet head. The parameters specifying the model are the same as those associated with the example in Fig. 3. Note that material flows upward after the head has contacted the sheet and begins to be squashed.

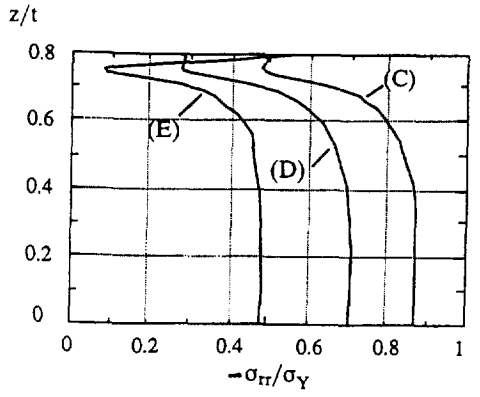

Fig. 7. Radial stress component acting normal to the shank/sheet interface at three stages of the loading process. See Eqn (2) for definitions of the stages (C)–(E). The parameters specifying the model are the same as those associated with the example in Fig. 3.

the sheet material to yield plastically in the vicinity of the hole. Contact between the head and sheet occurs when Δ is slightly in excess of δ. After contact, P increases sharply, and the average axial compressive stress at the mid plane of the shank peaks at almost $1.8\sigma_Y$ ((C) in Fig. 3(b)). This is the stage when the stress in the rivet head is increasing prior to attaining a level sufficient to begin

squashing the head. Lateral constraint of the sheets permits the development of a large component of hydrostatic pressure, $p = -\frac{1}{3}\sigma_{kk}$, superimposed on the state of uniaxial compression. Stress distributions across the mid-plane of the shank are plotted in Fig. 5 at (C), at an intermediate stage (D) when squashing of the head has begun, and in the limit state (E). The maximum axial compressive stress in the rivet occurs at stage (C) at the center of its mid plane. As the rivet head is deformed during the history between stages (C) and (E), both the compressive axial stress $-\bar{\sigma}$ and the hydrostatic pressure p in the shank *decrease* and asymptotically approach their values in the limit state. The limit load, $P \cong \pi R_H^2 \sigma_Y$, corresponds to the squashing load for the rivet head.

It can be seen from the differences between the undeformed and deformed meshes in Fig. 1 that the compressive axial strain in the central section of the shank is only about 5%, except at the corner where it meets the rivet head. If, in this example, the gap were closed by uniform compressive straining confined exclusively to the shank, the shank strain required would be about 33%. Instead, most of the deformation required to close the gap takes place in the vicinity of the rivet head and at the corner.

An explanation for the sharp drop in compressive axial stress and hydrostatic pressure in the shank of the rivet between stages (C) and (E) will now be given, as this drop is crucial to understanding the development of the clamping force. The state of high triaxial compression which develops in the shank of the rivet at stage (C) can only be contained as long as plasticity in the rivet head is confined to the central region just above the shank. As the load approaches $P \cong \pi R_H^2 \sigma_Y$, the rivet head undergoes general yielding as a squashing deformation with material flowing radially outward. Then, the highly compressed material in the shank flows out of the rivet hole into the head, substantially lowering the stresses in the shank to a level which can be contained by the plastically deforming head. This can be seen directly in Fig. 6 where the downward axial displacement at the center of the top of the shank where it meets the rivet head, $-u_z$, is plotted as a function of the driving displacement, Δ. Material at the top of the shank displaces monotonically downward until stage (C) is attained. Beyond this stage, between (C) and (E), a transient reversal occurs with the material flowing out of the rivet hole into the head. Most of the stress relief in the shank accompanying this reversed flow occurs over a relatively small range of Δ/δ (Fig. 6). For this particular example, the average compressive axial stress across the mid plane of the shank in the asymptotic limit state is approximately (*cf.* Fig. 3(b))

$$\bar{\sigma}_{\text{limit}} \cong -0.80\sigma_Y. \tag{3}$$

The calculations for this example were repeated with friction along the head-sheet interface modeled by Coulomb friction with a coefficient of unity. This change had virtually no effect on the results plotted in Fig. 3 nor on the limiting stress of Eqn (3). Including friction along the head-sheet interface also had no effect on the unloading response described next.

3.2. *The unloading process*

Let Δ be increased monotonically until $\Delta_{\max}$, and then decreased until P reaches zero. The unloading calculation is made anticipating that the interfaces between the rivet and the sheet remain closed, which is verified *a posteriori*. As mentioned in the statement of the model, sliding between the shank and the sheet is suppressed during unloading while the tangential traction between head and the sheet is taken to be zero. The unloading response is found to be strictly elastic producing no reversed plastic flow. Unloading at three different values of $\Delta_{\max}$ are shown as dashed lines in Fig. 3. Fig. 3(b) reveals that unloading to $P = 0$ takes place such that the slope of the normalized unloading curve is very nearly -1, i.e. the changes in $\bar{\sigma}$ and P satisfy $\Delta\bar{\sigma} \cong -\Delta P/(\pi R_H^2)$. Note that this slope would be exactly -1 if the sheet material outside the radius $r = R_H$ did not influence the unloading stress distribution. If that was the case, the stress change during unloading within the cylindrical region $r \leqslant R_H$ would be given precisely by the uniform uniaxial stress $P/(\pi R_H^2)$, where P is the load at $\Delta_{\max}$. The minimal role of the sheet material outside $r = R_H$ during unloading also clarifies why the sliding tractions on interfaces between sheet and the shank and head have little influence on the unloading stress changes: the stress change produces neither shear stress nor relative sliding on the interfaces in question. Thus, to very high accuracy, the *change* during unloading in the average axial stress across the mid plane of the rivet shank is

$$\Delta\bar{\sigma} = P/(\pi R_H^2). \tag{4}$$

3.3. *The residual clamping stress*

Combining the loading and unloading processes, one obtains the residual clamping stress as

$$\bar{\sigma}_{\text{residual}} = (\bar{\sigma})_{\Delta_{\max}} + P/(\pi R_H^2), \tag{5}$$

where $(\bar{\sigma})_{\Delta_{\max}}$ denotes the average shank stress at $\Delta = \Delta_{\max}$ when unloading is initiated. The curve for the small strain formulation in Fig. 4 is obtained using Eqn (5) together with the numerical data associated with the plots for the loading process in Fig. 3. The entire curve in Fig. 4 is generated by Eqn (5) from the single set of data for the loading process. For this example, the maximum residual clamping stress is approached asymptotically and is attained for practical purposes for $\Delta_{\max}/\delta$ somewhat greater than 1.5. The *asymptotic residual clamping stress* for the elastic–perfectly-plastic materials corresponds to the limit state. Using $P \cong \pi R_H^2 \sigma_Y$ for the limit load in Eqn (5), along with Eqn (3) for $(\bar{\sigma})_{\Delta_{\max}}$, one obtains as the asymptotic residual clamping stress

$$\bar{\sigma}_{\text{residual}} \cong 0.20\sigma_Y. \tag{6}$$

In the present example, no clamping force develops if $\Delta_{\max}/\delta$ is less than about 1.2 (Fig. 4). As $\Delta_{\max}/\delta$ is increased to 1.5 and larger, most of the loading displacement imposed by the frictionless platens on the rivet is accommodated by squashing of the rivet head. This is evident from the deformed mesh shown in Fig. 1.

It is worthwhile digressing at this point to emphasize why stress reversal in the shank during loading is crucial to understanding the origin of the clamping stress. The argument leading to $P/\pi R_H^2$ as the change in axial shank stress during unloading in Eqn (5) is valid independent of the stress history prior to unloading. As already noted, $P/\pi R_H^2 = \sigma_Y$, to an excellent approximation, once the rivet head experiences general yield. Therefore, by Eqn (5), it follows that average compressive stress across the mid-plane of the rivet shank prior to unloading at $\Delta_{\max}$ must be less than σ_Y if a residual tensile clamping stress is to exist. If the shank supported a *uniaxial compressive stress* σ_Y at $\Delta_{\max}$, the residual clamping stress would be zero.

Constraint supplied by the sheets on the lateral surface of the shank *increases* the average compressive stress in the shank to a value of about $1.8\sigma_Y$ prior to stress reversal (Fig. 3(b)). Were the rivet to be unloaded before stress reversal, there would be no clamping stress and, indeed, a gap would form between the rivet head and the sheets. In conclusion, stress reversal in the shank during loading is essential to the development of clamping stress. As already pointed out, stress reversal is a consequence of the multi-axial stress state in the shank, together with a partial release of the high hydrostatic compression when squashing of the head begins.

3.4. *Radial stress across the interface between shank and interface*

A substantial component of hydrostatic pressure exists across the shank at its mid-plane at the various stages of the loading process (Fig. 5(b)). The radial component of stress, σ_{rr}, acting on the interface between the rivet and shank at $r = R$ is plotted in Fig. 7 at three stages of loading. (The numerical resolution of this component of stress near the corner where the sheet, shank and head come together is poor. For this reason the plot is terminated at $z/t = 0.8$.) The trends are similar to those discussed in connection with Fig. 5. The compression along the interface is lowered due to relief of high triaxiallity when the rivet head starts to be squashed. However, even in the limit state, the radial compression acting on the interface is almost $\sigma_Y/2$. Since unloading produces only a uniaxial stress change, to a very good approximation, this radial compression represents the residual radial stress across the interface at the end of the riveting process in the unloaded state. It also follows that the residual compression acting across the interface will act to suppress any sliding during unloading, because little change in shear stress acting on the interface occurs during unloading.

3.5. *Finite strain modeling*

Several aspects of the results presented for the present example suggest that finite strain deformation effects might be important in the loading portion of the riveting process, and, therefore, in the development of the clamping stress. In particular, once contact takes place between the rivet head and the sheet, the head undergoes significant plastic deformation. For example, in Fig. 4 one notes that the development of the full clamping stress requires that $\Delta_{\max}/\delta$ be greater than 1.5. Because the initial gap δ in the example is $t/2$, the rivet head must be squashed by an additional $\approx 0.5\delta = t/4$ after the first contact occurs. As the initial thickness of the rivet head is $1.75t$, the squashing strain is

approximately 0.14. An associated increase of about 14% in the cross-sectional area of the head also occurs. While these are not large strains or geometry changes, they might be sufficient to produce a significant change in the predictions for the clamping stress. To assess the validity of the small-strain formulation, the calculations for the present example have been repeated using a finite-strain formulation as included in ABAQUS. The starting geometry is identical to that in the present example, and the sheet and rivet materials are again taken to be the same with yield stress σ_Y. The formulation fully updates geometry changes during the loading process and evaluates the stress changes during unloading starting from the deformed geometry at Δ_{max}.

A limit load does not exist in the finite strain formulation. Instead, as the rivet head is squashed, the load increases approximately as $\sigma_Y \pi R_H^2$ where R_H is the *current* radius of the head. Nevertheless, the residual clamping stress predicted by the finite strain analysis differs little from the prediction from the small strain formulation (Fig. 4). Even at $\Delta_{max}/\delta = 2$, corresponding to the head flattened to a thickness of about $0.75t$, there is only a 10% difference between the two predictions for the residual clamping stress. Insight into the agreement between the two formulations can be had from consideration of the two contributions in Eqn (5). Apart from the vicinity of the corner, the shank itself experiences relatively small strains, and it is reasonable to conclude that the average axial stress at the mid-plane of the shank at the onset of unloading is reasonably accurately predicted by the small-strain formulation. Secondly, the ratio $P/\pi R_H^2$ is the average normal stress applied to the surface of the rivet head, and this value is correctly estimated to be very nearly σ_Y in each of the two formulations, even though the difference in R_H can be fairly large. Thus, by Eqn (5), the residual clamping stress is well approximated by $(\bar{\sigma})_{\Delta_{max}} + \sigma_Y$. This argument is bolstered by the finding presented in the next section that the residual clamping stress is essentially independent of the size of the rivet head, as long as it is sufficiently large.

4. DEPENDENCE OF THE CLAMPING STRESS ON RIVET PARAMETERS

The model is used to explore the effect of several of the rivet parameters. Specifically, calculations are reported on the influence of the normalized gap size, δ/t; the size of rivet head; the ratio of rivet to sheet yield stresses; and strain hardening. All the result have been obtained using the small strain formulation.

4.1. *Initial gap size* δ

The initial gap size in the example reported in the previous section was one half the sheet thickness, $\delta/t = 1/2$. Figure 8 displays the dependence of the asymptotic (maximum) residual clamping stress as a function of δ/t. The other parameters specifying the initial geometry and materials are the same as those used in the example problem. In particular, the rivet and sheet materials are elastic–perfectly-plastic with a common yield stress, σ_Y. When δ/t is less than about 1/10, the clamping stress is negligible. The asymptotic residual clamping stress approaches a maximum of about $1/4\sigma_Y$ as δ/t approaches unity, which is the largest value for which calculations were

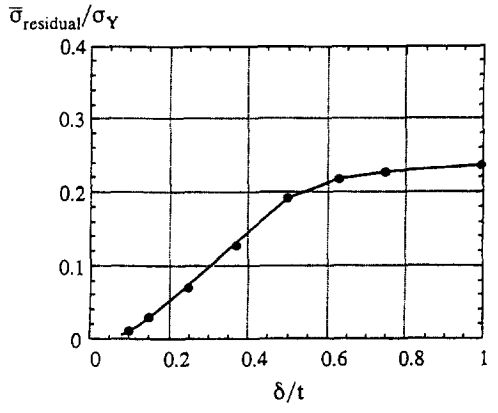

Fig. 8. Influence of the initial gap length δ on the asymptotic residual clamping stress. Identical rivet and sheet material properties with $\sigma_Y/E = 0.005$ and $\nu = 0.33$, and an undeformed geometry specified by $R/t = 2$, $R_H/t = 4$ and $t_H/t = 1.75$.

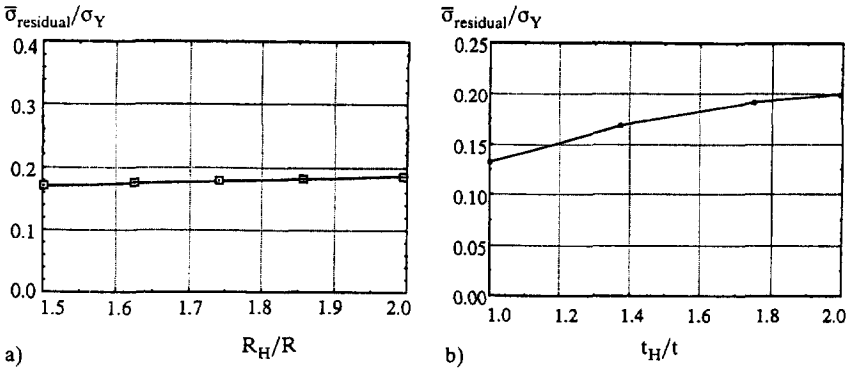

Fig. 9. Influence of the initial size of the rivet head on the asymptotic residual clamping stress. (a) Variation with respect to R_H/R with $t_H/t = 1.75$. (b) Variation with respect to t_H/t with $R_H/R = 2$. Identical rivet and sheet material properties with $\sigma_Y/E = 0.005$ and $\nu = 0.33$, and an undeformed geometry specified by $R/t = 2$ and $\delta/t = 1/2$.

performed. The increase in clamping stress with increasing gap size tends to level off for values of δ/t above about 1/2. Given the idealized nature of the symmetric double-headed rivet, it is difficult to draw conclusions for an actual single-headed rivet from the results in Fig. 8. Further insight would require a more realistic model of an unsymmetric rivet.

4.2. *Initial size of the rivet head*

The example problem had for the initial geometry $R_H/R = 2$, $R/t = 2$ and $t_H/t = 1.75$. Figure 9(a) shows the effect of reducing R_H/R on the asymptotic residual clamping stress, and Fig. 9(b) shows the effect of variations in t_H/t. Other than variations in R_H/R and t_H/t, the parameters characterizing the system are the same as those in the example problem. There is less than a 10% reduction in the asymptotic clamping stress resulting from a 25% reduction in the radius of the rivet head, from $2R$ to $3R/2$. For all practical purposes, the clamping stress is independent of the radius of the head for thicknesses above about $3R/2$, assuming the shank radius satisfies $R = 2t$.

The effect of varying the head thickness about the choice in the example problem, $t_H/t = 1.75$, is not insignificant. It appears that the asymptotic clamping stress levels out for t_H/t around 2, but there is a decided reduction in the clamping stress when t_H/t is reduced to unity.

In conclusion, the model suggests that for a system with $R/t = 2$, which is typical for many riveted sheet joints, the maximum clamping stress can be developed for a rivet head with radius $2R$ and thickness R. Here, again, the idealized nature of the model precludes definitive conclusions.

4.3. *Ratio of rivet to sheet yield stress, σ_Y^R/σ_Y*

The effect of the ratio of the yield stress of the rivet material to that of the sheet material, σ_Y^R/σ_Y, on the asymptotic clamping stress is shown in the two plots of Fig. 10. In the first of these plots [Fig. 10(a)], the clamping stress is normalized by the sheet yield stress, while in the second [Fig. 10(b)] it is normalized by the rivet yield stress. Both materials are elastic–perfectly-plastic, and all the other parameters have been taken to be the same as in the example problem. The yield stress of the sheet is fixed at $\sigma_Y/E = 0.005$. One sees immediately that the maximum asymptotic clamping stress for this example will never exceed $\cong 0.20\sigma_Y^R$, and this value is attained for values of σ_Y^R/σ_Y about unity. Moreover, with σ_Y held fixed, Fig. 10(a) reveals that reducing σ_Y^R/σ_Y below unity substantially reduces the clamping stress. Conversely, if σ_Y^R/σ_Y is increased above unity there is essentially no further increase in the clamping stress. Putting aside any influence of strain hardening, one can conclude that a rivet whose yield stress is equal to that of the sheet appears to provide as large a clamping stress as can be achieved.

4.4. *Strain hardening*

A limited study of the effect of strain hardening has been carried out for the special case where the rivet and sheet materials have identical properties. The tensile stress-strain curve used to

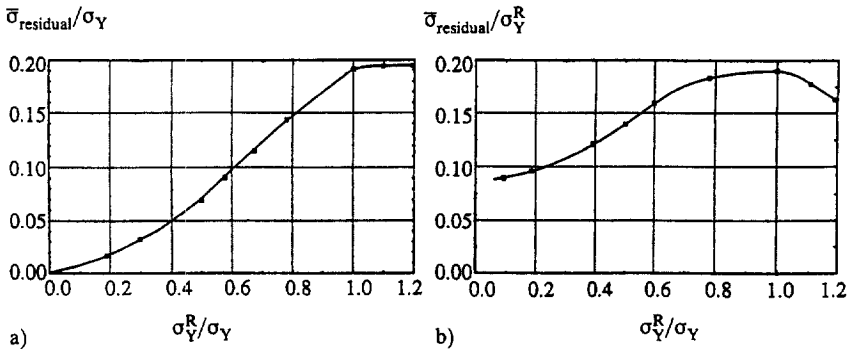

Fig. 10. Influence on the asymptotic residual clamping stress of the ratio of the yield stress of the rivet to that of the sheet, σ_Y^R/σ_Y, for elastic–perfectly-plastic materials. (a) Clamping stress normalized by yield stress of sheet. (b) Clamping stress normalized by yield stress of rivet. The sheet material properties are fixed at $\sigma_Y/E = 0.005$, and the undeformed geometry is specified by $R/t = 2$, $\delta/t = 1/2$, $R_H/t = 4$ and $t_H/t = 1.75$. Both materials have $\nu = 0.33$.

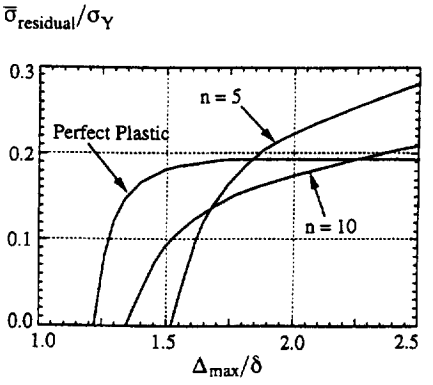

Fig. 11. The residual clamping stress versus Δ_{max}/δ for two levels of strain hardening and for an elastic–perfectly-plastic material. Identical rivet and sheet material properties with $\sigma_Y/E = 0.005$ and $\nu = 0.33$, and an undeformed geometry specified by $R/t = 2$, $\delta/t = 1/2$, $R_H/t = 4$ and $t_H/t = 1.75$.

characterize the material was taken to be the piecewise power law

$$\varepsilon = \begin{cases} \dfrac{\sigma}{E} & \text{for } \sigma < \sigma_Y, \\ \dfrac{\sigma_Y}{E}\left(\dfrac{\sigma}{\sigma_Y}\right)^n & \text{for } \sigma > \sigma_Y, \end{cases} \tag{7}$$

where σ_Y is now the initial yield stress and n the stress hardening exponent. The residual clamping stress as a function of Δ_{max}/δ for two levels of strain hardening is compared with the earlier result for the elastic–perfectly-plastic case in Fig. 11. The geometric parameters chosen for this comparison are identical to those used in the example problem, and the choices, $\sigma_Y/E = 0.005$ and $\nu = 0.33$, are also taken to be the same. When strain hardening is present, an asymptotic limit state and an asymptotic clamping stress no longer exist. The clamping stress increases monotonically with Δ_{max}/δ over the range for which the calculations have been carried out.

Values of the clamping stress greater than those predicted for the perfectly plastic system are obtained, but only at larger Δ_{max}/δ. Larger normalized clamping stresses in Fig. 11 are not surprising because σ_Y is the *initial* yield stress for the hardening materials, while it is the flow stress for the elastic–perfectly-plastic solids. Both the rivet and the sheet deform plastically, and thus both will strain harden above σ_Y. But the amount of straining in the rivet is quite different from that in the sheet, and, therefore, it is not a straightforward matter to relate the behavior in Fig. 11 to the perfectly plastic behavior due to differing yield stresses in Fig. 10. The main conclusion to be drawn

from the limited set of results in Fig. 11 is that, while strain hardening does not qualitatively change the mechanics underlying the development of the clamping stress, it appears to be quantitatively important.

5. CONCLUDING REMARKS

At the heart of the origin of the clamping stress in a cold-driven rivet is the release of the high hydrostatic pressure in the shank as the rivet head is squashed. The resulting average compressive stress in the shank prior to unloading has to drop below σ_Y if a residual clamping stress is to exist. The effect is all the more subtle because the residual clamping stress, $\approx \sigma_Y/4$, is small compared to the maximum compressive stress which develops in the shank during the riveting process, $\approx 2\sigma_Y$. The model enables the clamping stress to be computed as a function of the defining geometric and material parameters. Even for the model, the set of nondimensional parameters is surprisingly large: R/t, R_H/t, t_H/t, δ/t, σ_Y/E, σ_Y^R/σ_Y, n and n_R. In this paper, only the roles of R_H/t, t_H/t, δ/t, σ_Y^R/σ_Y and n have been considered. The advantage of invoking elastic–perfectly-plastic materials within the small-strain framework is the clarity accorded by the existence of the asymptotic residual clamping stress. Nevertheless, based on the limited study conducted here, strain hardening appears to be important, giving rise to a residual clamping stress which increases monotonically with respect to the maximum driving deformation, Δ_{max}. Indeed, Schijve's [2] experimental study reveals increases in lap joint fatigue life accompanying increases in riveter force, over the range of riveter force investigated. Further work with more realistic models will be needed to develop more refined predictions.

Acknowledgement—This work was initiated under support of FAA Grant 92-G-009 and completed with support of NSF-CMS-96-34632, and by the Division of Engineering and Applied Sciences, Harvard University. The authors are indebted to Dr. Matt Miller of the Boeing Company for supplying information on riveting processes.

REFERENCES

1. G. L. Kulak, J. W. Fisher and J. H. A. Struik, *Guide to Design Criteria for Bolted and Riveted Joints*, 2nd edn. Wiley, New York, 1987.
2. J. Schijve, Multiple-site damage fatigue of riveted joints. In *Durability of Metal Aircraft Structures*, eds S. N. Atluri, C. E. Harris, A. Hoggard, N. Miller and S. G. Sampath, *Proceedings of the Internationl Workshop on Structural Integrity of Aging Airplanes*, March 31–April 2, 1992. Atlanta Technological Publications, Atlanta, 1992.